Topology, Dynamics and Multifractal Analysis of Turbulence near a Turbulent/Non-Turbulent Interface

Rui Manuel Marques Jaulino
rui.jaulino@ist.utl.pt

Instituto Superior Técnico, Lisboa, Portugal

December 2014

Abstract

Two universal aspects of turbulence, the distribution of the invariants of the velocity gradient tensor and the multifractal spectrum of dissipation, are analysed near a Turbulent/Non-Turbulent Interface using Direct Numerical Simulations of shear-free turbulence.
The invariants of the velocity gradient tensor provide only local information, in contrast to eddy structures which necessarily involve data from a given flow region. We show that in a turbulent/non-turbulent interface, such as exists at the edges of wakes and jets, the invariants show the imprint of the small scale eddies from the nearby turbulent region, and can be described by a simple model relating local flow topology, dynamics and eddy structure, thus unifying the previous models for the viscous superlayer and the turbulent sublayer within the Turbulent/Non-Turbulent Interface.
The recent result of non-conservativeness of the multiplicative cascade which describes the energy dissipation is obtained with the Wavelet Leaders method by analysing the flow both in the turbulent region and in the Turbulent/Non-Turbulent Interface. The present results on the multifractal spectrum of dissipation imply that the previous results in the literature on the fractal dimension of the Turbulent/Non-Turbulent Interface need to be revisited. **Keywords:** Turbulence, T/NT Interface, Multifractal Analysis

1. Introduction

In the real word turbulence is omnipresent, found in almost all natural flows, industrial processes and engineering applications, and is probably the most challenging problem of fluid mechanics. Turbulence is Nature's way of speeding up diffusion, transport and mixing in fluids by the generation of self-similar multiscale motions.

1.1. Turbulent/non-Turbulent Interface

In turbulent shear flows, such as jets, shear layer growth is promoted by the interaction between turbulent and non-rotational flow lying at opposite sides of the turbulent shear layer boundary, in a process denominated as *Turbulent Entrainment*. This entrainment process is characterized by significant exchanges of mass, momentum, passive or active scalars, like concentration or temperature, and energy across a thin layer of turbulent fluid known as Turbulent/Non-Turbulent Interface.
Fluid outside the interface, which is initially irrotational acquires vorticity in one of two ways: either by *engulfment* where there are large scale convolutions of the interface with negative curvature pointing inward or by *nibbling* along the entire interface by a viscous diffusion process.
The vorticity build up mechanism across the TNTI is governed by two distinct mechanisms according to the different nature of the two layers that composes the TNTI [1]:

- at the so called, *viscous super-layer* (VSL), which is an external layer, close to the irrotational zone, where viscous processes dominate the entrainment - diffusion of enstrophy;
- whereas in the *turbulent sub-layer* (TSL), where enstrophy production and vortex stretching dominates the entrainment.

From the geometrical point of view the interface is a very complex object with fractal characteristics [2].

1.2. Objectives

The present thesis is devoted to the investigation of fundamentals in turbulence related to the universal turbulent characteristics within free shear layers which constitute canonical prototypes for fundamental turbulence research being the goal of this work twofold: to investigate the evolution of the small scale universal features at Turbulent/Non-

Turbulent Interfaces, as exists in jets, wakes, mixing layers and boundary layers, and to develop and apply multifractal tools in this context.

2. Background

2.1. Invariants of the Velocity Gradient Tensor

The study of the invariants of the velocity gradient tensor present a clear geometric interpretation and results based on these quantities shown some universal characteristic of turbulence.
By calculating the invariants of $A_{ij} = \frac{\partial u_i}{\partial x_j}$ in any flow, we can obtain information regarding the local geometry because we have information of how the elements near a certain point are moving [3].
As will be shown below, the characteristic equation of the velocity gradient tensor A_{ij}, equation 1, determines the type of trajectories.

$$\lambda_i^3 + P\lambda_i^2 + Q\lambda_i + R = 0 \tag{1}$$

where λ_i are the eigenvalues of A_{ij} and P, Q and R are the invariants of A_{ij}. Since $P = 0$ in incompressible flows the other two invariants are usually analysed in a joint probability distribution map (Q, R map). Here, depending on the location, the ideas presented can be associated with zones in this map (figure 1).

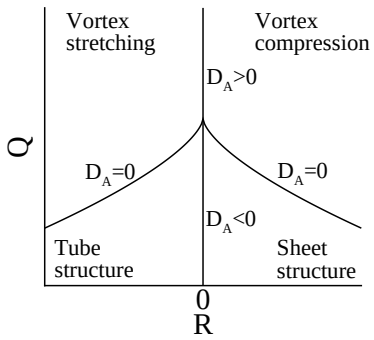

Figure 1: Interpretation of the Q, R map.

The (Q, R) map (figure 1) allows to *infer* about the relation between the local flow topology (enstrophy or strain dominated) and the enstrophy production term (vortex stretching or vortex compression).
In many turbulent flows the (R, Q) map displays a correlation between R and Q in the region $R < 0, Q > 0$ associated with a predominance of vortex stretching and a strong (anti) correlation between R and Q is present in the region $R > 0, Q < 0$ associated with sheet like structures.

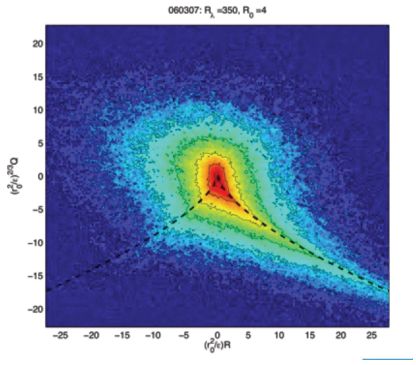

Figure 2: Typical Q, R map observed in turbulence.

This gives the (Q, R) map its characteristic "teardrop" shape that has been observed in a great variety of different turbulent flows such as isotropic turbulence, mixing layers and channel flows.

2.2. Fractals

A fractal (from the Latin word *fractus*, which means broken or fractured) can be defined as fragmented geometric shape which can be split into parts that are a scaled copy of the whole. While a fractal is a strictly mathematical construction, it is found in various non-mathematical models such as natural systems.
To understand fractals, it is important to know what their characteristics are. Its first characteristic is that its structure is defined by fine and small scales and substructures. Another characteristic is that its shape cannot be defined with Euclidean geometry. In addition it is recursive and shows iteration to some degree. In addition, fractals are informally considered to be infinitely complex as they appear similar in all levels of magnification.
Studying fractals is both a complicated yet interesting branch of mathematics, and, despite all its intricacies, it proves itself a useful tool.

2.2.1 Fractal Dimension

The fractal dimension of a given object can be defined as [4]:

$$d_f = \lim_{l \to 0} -\frac{\log(N(l))}{\log(l)} \tag{2}$$

where $N(l)$ is the number of elements of size l needed to cover the object. In practical terms d is the slope of $\log(N(l))$ versus $\log(l)$. This definition gives the euclidean dimension for regular objects.
A common example of a fractal object is the *Koch curve*. It is the limit of the iterative process represented in figure [3].

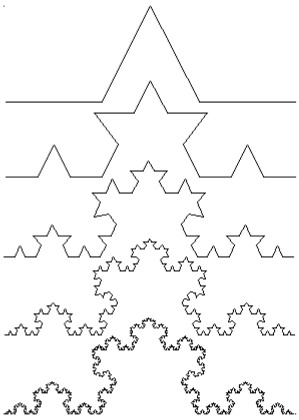

Figure 3: The Koch curve. This object is generated iteratively by replacement of the *straight* lines with the original object (at each iteration).

To determine it's fractal dimension one only has to notice that, in the top of the figure (the shape that is successively reproduced) are needed 4 elements with length $\frac{1}{3}$. In the next iteration it is composed of $16 = 4^2$ elements of length $\frac{1}{9} = \frac{1}{3^2}$. In some iteration k, this idea can be generalized and so one has 4^k elements with length $\frac{1}{3^k}$. Then by equation [2] is possible to obtain that the fractal dimension of the *Koch curve* is just $d_f = \lim_{l\to 0} -\frac{\log(N(l))}{\log(l)} = \lim_{k\to\infty} -\frac{\log(4^k)}{\log(\frac{1}{3^k})} = \frac{\log(4)}{\log(3)} = 1.26$.

2.3. Multifractals

Multifractal systems are common in nature. They include fully developed turbulence, stock market time series, real world scenes, the Suns magnetic field time series, heartbeat dynamics and natural luminosity time series.
In a multifractal system, the behaviour near any point x can be described as [4]:

$$f(x+l) - f(x) \sim l^{h(x)} \tag{3}$$

where $h(x)$ is the holder exponent at the point x which can interpreted as a generalization of the notion of Taylor series. Hence any function can be expanded as a Taylor series where the exponent h is present in the higher order term i.e, $f(x) = a_0 + a_1 x + \cdots + a_h x^h$.
The fundamental quantity that characterizes a multifractal is the *multifractal spectrum*, $D(h)$. Typically $D(h)$ is bell-shaped [4 and it can be interpreted in geometrically.

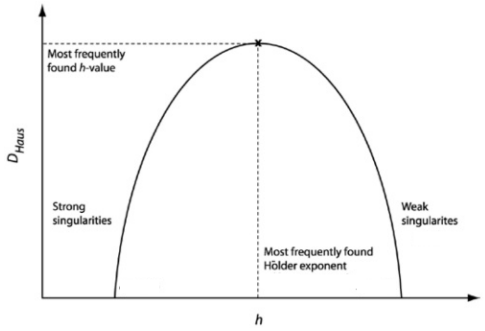

Figure 4: Typical example of a multifractal spectrum.

$D(h)$ represents the fractal dimension of the set of intervals where the holder exponent is h; since h can take any value between h_{min} and h_{max} there are an infinite number of fractal sets residing within the same set - hence the term *multifractal*.

2.3.1 The Multifractal Formalism

Characterizing the multifractal spectrum from it's definition is an almost impossible task - it would involve the determination of the point wise singularity exponent for every point in the function. To overcome this issue the multifractal formalism was developed allowing to determine the multifractal spectrum from quantities that are relatively easy to compute.
Parisi and Frisch in [5] developed a multifractal formalism to study the behaviour of velocity increments in fully-developed turbulence (a key quantity in Kolmogorov's theory). The idea was to study asymptotic power law behaviour of moments of velocity increments, when the distance $l \to 0$ (here it should be considered the velocity signal as a $1D$ function). Mathematically this is done by defining the *structure function* $S(l,q)$ as

$$S(l,q) = \frac{1}{n(l)} \sum_{x_0} |f(x_0 + l) - f(x_0)|^q \tag{4}$$

where $n(l)$ is the number of points separated by a distance l. The quantity τ_q is called *scaling function* and it is defined as

$$\tau_q = \lim_{l\to 0} \frac{\log S(l,q)}{\log(l)} \tag{5}$$

To determine $D(h)$ the following relation holds

$$D(h) = \min_q (1 - \tau_q + qh) \tag{6}$$

In reference [6], the multifractal spectrum is associated with a measure $\mu(x)$ which is a function that assigns a value to an interval of the space. For each

point x a *local singularity exponent* $\alpha(x)$ is defined as (in analogy with the holder exponent)

$$\alpha(x) = \lim_{l \to 0} \frac{\log(\mu(I_l))}{\log(l)} \tag{7}$$

where I_l is the interval where the measure is defined. In the same vein as in the definition of the multifractal spectrum, it is possible to define the so called *singularity spectrum* $f(\alpha)$ as the fractal dimension of the set where the singularity exponent is α. An analogue to the structure function defined in [4] is

$$S_m(l, q) = \int_{\mathbb{R}} \mu(B_l(x))^q d\mu(x) \tag{8}$$

where $B_l(x)$ is the ball of radius l centred in x. A scaling exponent τ_q^M can be defined as (in analogy with τ_q)

$$\tau_q^M = \lim_{l \to 0} \frac{\int_{\mathbb{R}} \mu(B_l(x))^q d\mu(x)}{\log(l)} \tag{9}$$

The analogy between τ_q and τ_q^M can be made [7]; if one works in one dimension, is easy to note that $B_l(x) = [x - l, x + l]$, and then τ_q can be rewritten as

$$\tau_q = \lim_{l \to 0} \frac{\log(\int_{\mathbb{R}} |\psi(x + l) - \psi(x - l)|^q d\mu(x))}{\log(l)} \tag{10}$$

where

$$\psi(x) = \int_{-\infty}^{x} d\mu(y) \tag{11}$$

Then τ_q and τ_q^M have the same meaning if one considers the cumulative integral of the measure under study. Another point of interest is the following: if one considers the holder and the scaling exponents is possible to conclude from the previous analogy that $\alpha = h+1$; by integration of the measure trough equation 11 we are increasing the exponent in one (for one dimension) and so $\tau_q^M = \tau_q + dq$.

2.3.2 Multifractal Processes

The binomial cascade is one the simplest process to exhibit multifractal properties. This (iterative) process starts with the unit interval $I_0 = [0, 1]$, where a constant mass is assigned, divides it into consecutive smaller pieces and at the same time divides the mass attributed at each smaller interval.
The iteration begins with a uniform distribution $\mu_0[0, 1] = m_0$ (with $0 < m_0 < 1$), subdivides it into a distribution with $\mu_1[0, \frac{1}{2}] = m_0$ and $\mu_1[\frac{1}{2}, 1] = m_1 = 1 - m_0$, further subdivides it into $\mu_2[0, \frac{1}{4}] = m_1 m_1$, $\mu_2[\frac{1}{4}, \frac{1}{2}] = m_0 m_1$, $\mu_2[\frac{1}{2}, \frac{3}{4}] = m_0 m_1$ and $\mu_2[\frac{3}{4}, 1] = m_0 m_0$ and so on. As shown in figure 5, successive iterations of this produces a multiplicative cascade that generates an infinite sequence of measures whose limit measure is the binomial cascade.
The scaling exponent is given by

$$\tau_q^M = -\log_2(m_0^q + m_1^q) \tag{12}$$

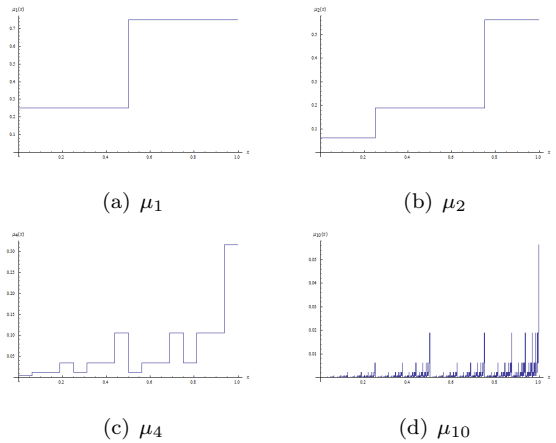

(a) μ_1 (b) μ_2

(c) μ_4 (d) μ_{10}

Figure 5: The generation of the binomial measure with ($m_0 = 0.25$), μ_i, where i is the number of the iteration - from *The Wolfram Project*

2.3.3 Turbulence Energy Cascade as a Multiplicative Process

In 1962 Obukhov proposed that the 1941 Kolmogorov theory should be generalized to include the fluctuations in the mean dissipation. In particular, he suggested that the velocity structure functions should consider the manner at which ε varies locally. This yields

$$S_p(r) = < |u(x+r) - u(x)|^p > \sim < \varepsilon_r^{p/3} > r^{p/3} \tag{13}$$

where $\varepsilon_r(x)$ is the mean dissipation over a domain of size r. The key issue should be to understand how ε_r behaves and to understand the moments $< \varepsilon_r^q >$ with some kind of mechanism. Evidences of multifractal behaviour of ε_r (i.e, deviation from a pure fractal, like the previous examples) where shown in [8]. This picture of the energy viscous dissipation as a multiplicative process originated from the argument of the energy cascade.
A vital ingredient is the concept of a measure density which, in the present context, is the rate of dissipation per unit volume ε_r. Establishing an analogy between the total dissipation E_r, in a certain piece Ω of size r, $E_r = \int \varepsilon(x) dx$, when a piece Ω decays into smaller ones, each smaller piece can be thought of as receiving a fraction of E_r. The local singularity exponent in agreement with equation 7 is defined as:

$$\frac{E_r}{E_L} \sim \left(\frac{r}{L}\right)^{\alpha} \tag{14}$$

or,

$$\frac{\varepsilon_r}{\varepsilon_L} \sim \left(\frac{r}{L}\right)^{\alpha - d} \tag{15}$$

where d is the euclidean dimension of the support of the measure.
Following the reasoning outlined for the study of multifractals one can describe the process by it's moments,

$$\sum E_r^q \sim E_L^q \left(\frac{r}{L}\right)^{\tau_q^M} \tag{16}$$

and define the [Hent procc] generalized dimensions D_q as

$$D_q = \frac{\tau_q^M}{q-1} \tag{17}$$

With this underlying picture, reference [8] and [9] observed that a binomial cascade with $m_0 = 0.3$ agrees with the behaviour of dissipation in several flows and conjectured that D_q and $D(h+1)$ should be universal parameter in turbulence.

2.3.4 Fractal Dimension of T/NT Interface

An estimation of the fractal dimension of the T/NT Interface is present in reference [2]:

$$d_f = \frac{7}{3} + \frac{2}{3}\left(3 - D_{1/3}\right) \tag{18}$$

where $D_{1/3}$ is the generalized dimension at $q = 1/3$. This result depends on the multifractal spectrum of the dissipation in the interface.

2.3.5 Practical Multifractal Analysis

Wavelets have been used for a long time to study scaling behaviour and irregularity of functions [10]. It can be proven [11] that a partition function based on the discrete wavelet coefficients of the function can be used to determine the multifractal spectrum.

$$Z_d(j,q) = \frac{1}{2^j}\sum_k d(j,k)^q \tag{19}$$

where $d(j,k)$ are the wavelet coefficients at position k and scale j. Also $Z_d(j,q)$ scales as

$$Z_d(j,q) \sim 2^{j\tau_q} \tag{20}$$

and so a reasoning identical to equation 6 is valid [11].

3. Direct Numerical Simulations and Post-Processing Tools

3.1. Shear-Free Turbulence

The present work makes use of direct numerical simulations (DNS) of shear free turbulence in a periodic box with sizes 2π with 512^3 collocation points[12]. The simulation starts by instantaneously inserting a velocity field from a previously run DNS of forced isotropic turbulence into a field of quiescent fluid. The initial isotropic turbulence region then spreads into the irrotational region in the absence of mean shear, developing a distinct TNTI layer. In the present shear free simulation the Reynolds number based on the Taylor micro-scale is equal to $Re_\lambda \approx 115$ and the resolution is $\Delta x/\eta \approx 1.5$. Details can be found in [12] and references therein.

3.1.1 Conditional Statistics

Conditional statistics of several quantities with respect to the distance from the TNTI have been employed in recent works [1] and the procedure to obtain them is only briefly described here. The location of the outer edge of the TNTI is defined by the surface where the vorticity magnitude is equal to a certain threshold $\omega = \omega_{tr}$, whose level is obtained from topological considerations as described in reference [1] and above. The conditional statistics are then computed as function of the distance y_I to the TNTI layer using one of three possible orientations to the interface (see Fig. 6): *i)* 'vertical' to the TNTI *i.e.* parallel to the y-axis (1D), normal to the TNTI projected into the (x,y) plane (2D), or normal to the TNTI (3D). In the resulting conditional mean profile the TNTI is by definition located at $y_I = 0$, while the irrotational and turbulent regions are defined by $y_I < 0$ and $y_I > 0$, respectively, where y_I is normalised by the Kolmogorov micro-scale in the turbulent region $\eta = \eta(y_I \gg 0)$ [12].

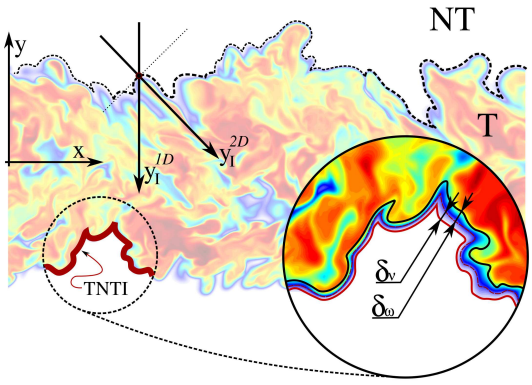

Figure 6: Local coordinate systems used to compute the conditional mean profiles.

3.2. Wavelet Leaders

Instead of building the structure function as in equation 19 with the discrete wavelet coefficients, those are replaced by a quantity derived from them called the *Wavelet Leaders*.
The Wavelet Leaders, $L(j,k)$, are defined as the maximum of the wavelet coefficients, $d(j,k)$, in a certain modified dyadic interval $I_3 = [(k-1)2^{j_i}, (k+2)2^{j_i}]$, where all the scales below the one in study are considered (i.e for every $j_i \leq j$). The scaling function is determine by the slope of the curves

$\log(Z_L(j,q))$ versus $\log(2^j)$ and the multifractal spectrum follows from it's definition.

4. Results

4.1. Flow Topology near a Turbulent/Non-Turbulent Interface

Figure [7] details the enstrophy build up mechanisms across the TNTI by plotting conditional mean profiles of vorticity magnitude ω, enstrophy viscous diffusion $\nu\partial^2(\omega_i\omega_i/2)/\partial x_j\partial x_j$, and enstrophy production $\omega_i\omega_j s_{ij}$, for the present DNS.

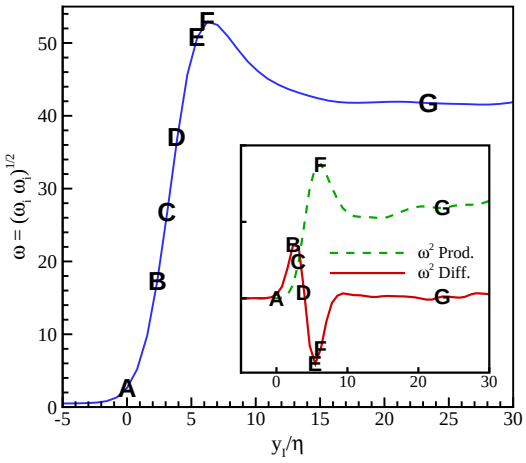

Figure 7: Mean conditional profiles (as function of the distance from the TNTI) of vorticity magnitude ω, enstrophy production (ω^2 Prod.) and enstrophy viscous diffusion (ω^2 Diff.).

Several letters (**A-G**) are assigned to specific locations within the TNTI, where **A** denotes the start or the 'outer edge' of the TNTI (i.e. the origin of the local reference frame $y_I = 0$). The viscous diffusion exhibits a characteristic shape with positive/negative maxima at $y_I/\eta = 2.4$ (**B**) and $y_I/\eta = 5.5$ (**E**) associated with gain/loss of enstrophy, respectively, as previously reported by several authors[1], being clear that this is the mechanism triggering the enstrophy rise observed inside the TNTI [12]. The diffusive transport switches signal between the two extrema crossing zero at $y_I/\eta = 3.9$ (**D**). On the other hand the enstrophy production becomes important after $y_I/\eta \approx 2$ but by $y_I/\eta \geq 3.1$ (**C**) is already the main responsible for the enstrophy amplification surpassing the viscous diffusion. The conditional mean enstrophy exhibits a sharp rise between $0 \leq y_I/\eta \leq 6.3$ (**A-F**) until by $y_I/\eta = 6.3$ (**F**) the maximum enstrophy is attained. By $y_I/\eta = 23.5$ (**G**) the flow exhibits all the characteristics of fully developed turbulence, with no sign of the presence of the TNTI.

Therefore, in the present case the VSL, associated with the viscous diffusion of vorticity towards the irrotational flow region [12], extends from $0 \leq y_I/\eta \leq 3.1$ (**A** to **C**), *i.e.* with a mean thickness (defined by the region in Fig. 7 where diffusion exceeds production), equal to $\langle\delta_\nu\rangle \approx 3\eta$, while the TSL (associated with the rapid vorticity rise by vorticity production) lays between $3.1 \leq y_I/\eta \leq 6.3$ (**D** to **F**), with an estimated mean thickness (region where production exceeds diffusion culminating in the maximum vorticity - figure 7) equal to $\langle\delta_\omega\rangle \approx 3\eta$. Thus in the present flow both $\langle\delta_\omega\rangle \sim \langle\delta_\nu\rangle \sim \eta$ in agreement with reference [12]. The mean thickness of the VSL $\langle\delta_\nu\rangle$ was estimated (Corrsin and Kistler) to be of the order of the Kolmogorov micro-scale since the physical process within this layer is the viscous diffusion of vorticity from the turbulent core into the irrotational region this process should be solely controlled by the amount of vorticity in the turbulent region ω' and by the molecular viscosity ν. On dimensional grounds it follows that the characteristic length scale for this process, defined as the thickness of the VSL, is $\delta_\nu = \delta_\nu(\nu,\omega')$, leading to $\delta_\nu \sim (\nu/\omega')^{1/2} \sim \left(\nu^3/\varepsilon\right)^{1/4} \sim \eta$, where ε is the mean rate of viscous dissipation in the core of the turbulent region.

The development of the 'teardrop' shape across the TNTI can be appreciated by plotting the joint pdfs of R and Q at several fixed distances from the TNTI layer and describes how an initially Non-Turbulent fluid element becomes Turbulent. Fig. 8 shows the pdfs in the VSL (at $y_I/\eta = 0$, 2.4 and 3.1 - **A-B-C**) while Fig. 9 shows the pdfs in the TSL (at $y_I/\eta = 3.9$, 5.5, and 6.3 - **D-E-F**).

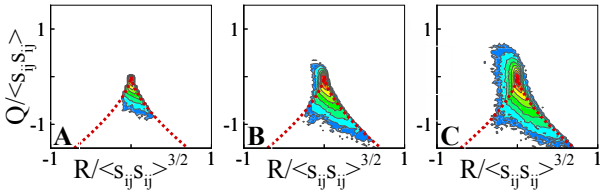

Figure 8: Joint probability density function of R, Q across the viscous-superlayer (VSL) region in the flow: start of the viscous superlayer (**A**), point of maximum mean enstrophy diffusion (**B**), end of the viscous superlayer (**C**).

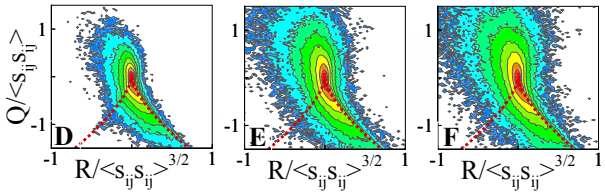

Figure 9: Joint probability density function of R, Q across the turbulent sublayer (TSL) region in the flow: point of zero diffusion (**D**), point of minimum diffusion (**E**), point of maximum enstrophy (**F**).

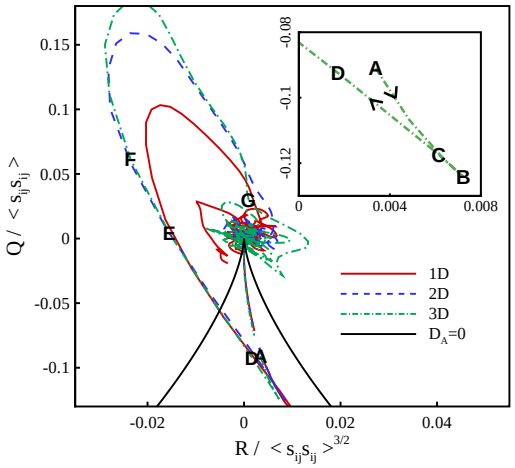

Figure 10: Trajectory of the mean values of R and Q across the TNTI. $D_A = 27/4R^2 + Q^3$ is the discriminant of the eigenvalues of A_{ij}.

The VSL is predominantly linked with the formation of the 'teardrop' shape in the 4th quadrant, associated with a predominance of sheet structures. Since the VSL is at the edge of the eddies from the T region[12], strain dominates over enstrophy, and $R > 0$ (sheet structures) is more frequent than $R < 0$ (tube structures). In contrast in the TSL the formation of the 'teardrop' shape occurs in the 2nd quadrant with the enstrophy now overcoming strain, thus $Q \approx \omega_i\omega_i/2 > 0$ and $R \approx -\omega_i\omega_j s_{ij}/4$. The predominance of the non-linear over the viscous mechanisms implies that the only way the enstrophy can grow is when ω_i and s_{ij} are correlated so that $\omega_i\omega_j s_{ij} > 0$, *i.e.* more frequent events of $R < 0$ (vortex stretching) than $R > 0$ (vortex compression). The increasing intensity of R and Q as one moves from **A** to **F**, naturally reflects the increasing intensity of the fluctuating fields of enstrophy and strain. The results are in agreement with the conditional profiles displayed in Fig. 7. It is noteworthy that in contrast with the jet (where the 'teardrop' forms in $\langle\delta_\omega\rangle \sim \lambda$), here, the 'teardrop' shape develops in a much shorter distance, requiring only $\approx 5.5\eta$ to form completely. Indeed, the joint pdf of (R, Q) at **E** is virtually identical to **F** and also **G** (not shown).

A very interesting perspective of the formation of the teardrop is provided by the trajectory of the (conditional average of the) invariants of the velocity gradient tensor in the (R, Q) map, obtained from the conditional mean profiles using the three different orientations (1D, 2D and 3D), presented in Fig. 10.

Only in the 2nd quadrant do we observe some differences in the statistics which shows the robustness of the conditional statistics. The T region is mainly in the 2nd but also in the 1st quadrants. There is an increasing tendency for finding a sheet topology as the fluid particles enter the VSL (**A** to **C**), followed by a sharply increased predominance of vortex stretching and formation of tube structures as the flow evolves inside the TSL (**C** to **F**), in agreement with the model for the VSL proposed in reference [12]. Interestingly, the trajectory connecting the VSL and TSL regions (**B** to **E**) consists in a straight line with a (constant) slope which is the same for all the three orientations used in the conditional statistics (1D, 2D and 3D).

It is possible to explain the result present in figure 10 by recalling that the small scale eddies ('worms') determine the TNTI characteristics. Recently, using the Burgers vortex which is a good model for the small scale eddies in turbulent flows, it has been shown that the periphery and core of the eddies existing near the TNTI determines the thickness of both the VSL and TSL [1],[12]. Interestingly, resorting to the analytical radial profiles of $Q(r)$ and $R(r)$ for a Burgers vortex one can derive a linear relationship between the invariants: $Q(r) = -R(r)/\gamma_B - \gamma_B^2$, where γ_B is the axissymmetric strain created by the axial velocity $u_z(z) = \gamma_B z$ imposing the vortex core radius $R_B = 2\left(\nu/\gamma_B\right)^{1/2}$. Recalling that a typical small scale eddy from inside the turbulent region has a vortex core radius equal to $R_{ivs}/\eta \approx 5$ [13], the strain rate imposed on this eddy can be estimated as $\gamma_{ivs} = 4\nu/R_{ivs}^2 = 5.9$. On the other hand, by measuring the slope of the straight line in the (R, Q) trajectory from **B** to **E** in Fig. 10 we arrive at a stretching rate of $\gamma = 5.5$, which is remarkably

close to the value obtained assuming the flow in the VSL and TSL is described by a Burgers vortex. Thus, the (R, Q) trajectory shows the imprint of the small scale eddies existing near the TNTI, and unifies the existing models for the VSL and TSL within a TNTI. The small differences obtained with the three orientations in the 2nd quadrant can now be explained: the 1D orientation will less likely align with the radial direction of the eddies forming the TNTI than the 3D orientation (because the vorticity is larger in the core of the eddy), thus explaining why the straight line linking the VSL and TSL is longer for the 3D than for the 1D orientation. Both the 'tear-drop' formation and mean trajectory of (R, Q) are expected to hold in other flows *e.g.* fully developed wakes and jets, since the VSL forms at the edge of similar small scale eddies in these flows[12].

4.2. Multifractal Analysis of Turbulence

4.2.1 Dissipation in Fully-Developed Turbulence

The dissipation was analysed using DNS data from fully-developed turbulence for several 2D planes of the simulation.
In figure 11 is possible to observe that the scaling exponents are very similar in all planes. This is an indication of statistical convergence.

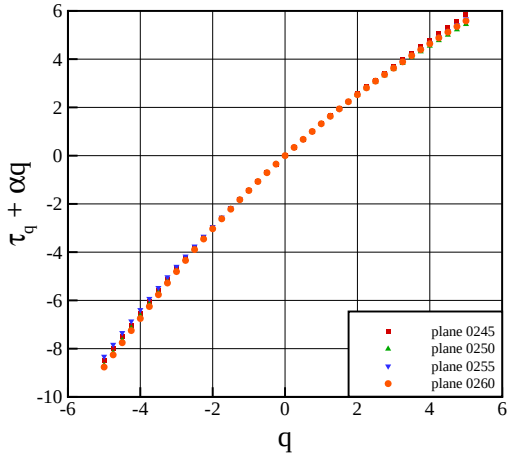

Figure 11: Scaling exponents obtained in different planes.

The obtained multifractal spectrum is shown in figure 12. In the same figure several models proposed are represented for comparison: the model in reference [8] - binomial cascade with $m_0 = 0.3$ - is represented by a dash-dotted red line and the model in reference [14] - binomial cascade with $m_0 = 0.36$ and $m_1 = 0.78$ - is represented by a dashed blue line. A proposed model of our own to fit the obtained data is represented by a solid black line - binomial cascade with $m_0 = 0.4$ and $m_1 = 0.75$.

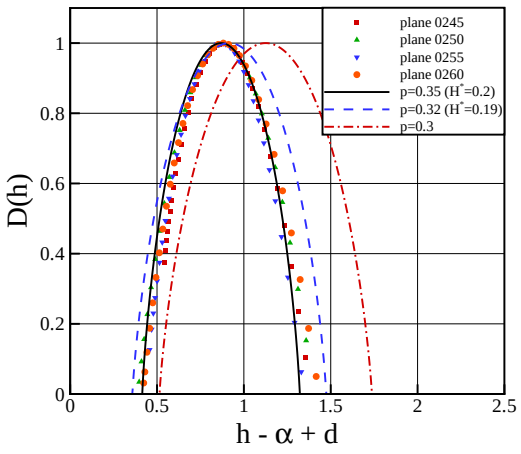

Figure 12: Multifractal spectrum obtained in different planes in comparison with several models proposed.

It can be observed, in the first place, that for all the planes in the turbulent zone analysed, the data collapses with each other. Another important aspect is that the cancellation exponent (see [14]) is different from zero. This is an indication that the main conclusion of [14] is observed again: if the dissipation is to be modelled as a multiplicative cascade, this cascade is not conservative - $(m_0 + m_1 \neq 1)$. Nevertheless it can be observed that the model proposed in [14] does not agree with our results for the negative exponents (right part of $D(h)$) because the negative q values are associated with the weakest singularities and in [14] the data is filtered we can conjecture that this is the reason for the differences in the negative exponents (and they need to filter the data in order to make their method work. We obtain this same behaviour with a method different from the WTMM that is used in [14]). Since there is also some ambiguity in the choice of the scaling range, we can say that only by biasing the results one could match the results in [14]. Nevertheless the results obtained are in relatively good agreement.
Another important conclusion about non conservativeness of the cascade is that if one considers a conservative binomial cascade and fractionally integrates it by a factor of , say, H^* one can obtain a function that is also a multiplicative process but with some degree of regularity [14]. In our case, a conservative cascade with $m_0 = \frac{0.4}{0.4+0.75} \approx 0.35$ will have a multifractal spectrum equal to the one obtained with the non conservative model but it is shifted to the left by a factor of $H^* = \log_2(0.4 + 0.75) \approx 0.2$.
This result can have a very simple interpretation: since the Reynolds number is finite the function will have some degree of regularity below a given scale

(in this case the Kolmogorov micro-scale) and so it must be expected that, if the process is a pure multiplicative one (in the limit of infinite Reynolds) it must display some kind of behaviour of this type. This result cannot be achieved with box counting method because by construction this method always yield a conservative cascade even if it is not the case [14].
The generalized dimensions for our data (according to the model which agrees better with the results) are given by

$$D_q = \frac{-\log_2(0.4^q + 0.75^q)}{q-1} \tag{21}$$

4.2.2 Dissipation near the T/NT Interface

The dissipation was also analysed by using data conditioned to the distance to the interface. In figure 13 is represented the scaling functions obtained; it is also shown for comparison a scaling function for one the planes in the turbulent zone.

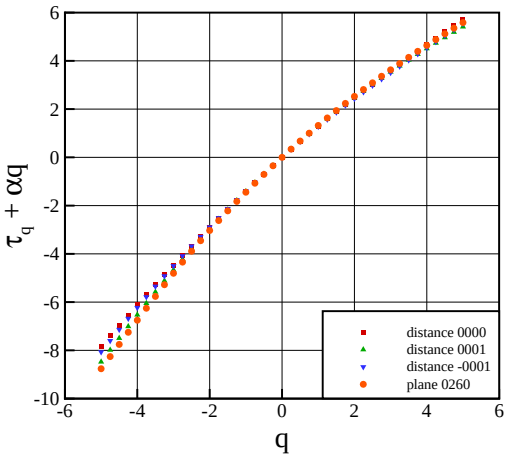

Figure 13: Scaling exponents obtained for different distances.

It can be observed that the scaling functions in the interface are very similar to those in the turbulent zone.
With respect to the multifractal spectrum the results are present in figure 14. The comparative models shown are the same as in figure 12.

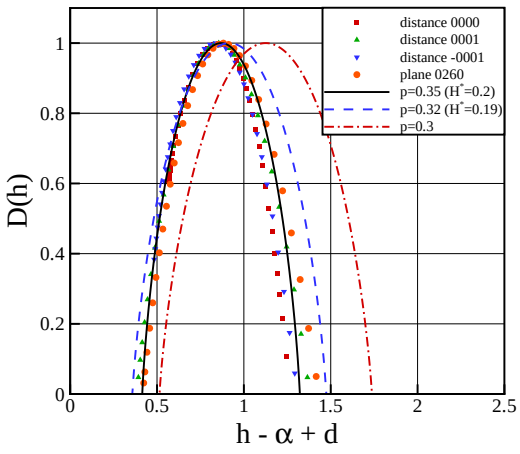

Figure 14: Multifractal spectrum obtained for different distances.

It can be observed that, for this simulation, there is evidence that the multifractal spectrum in the interface is similar to the spectrum in the turbulent zone and the same comments apply to this case.
If one recalls equation 18 and establishes and analogy, since we determined the multifractal spectrum for one dimensional signals, we have

$$d_f = \frac{7}{3} + \frac{2}{3}\left(1 - D_{1/3}\right) \tag{22}$$

From equation 21 one can calculate that $D_{1/3} \approx 1.0776$ and predict, with this results, $d_f \approx 2.28$. This value is slightly lower that the value predicted from [8] where $d_f \approx 2.36$. Remembering that the cascade is non conservative, the value of the fractal dimension should indeed be lower.
This is a very interesting result since, as shown in reference [15], experimentally it was obtained that the fractal dimension of the interface was $d_f = 2.37$ consistent with a value slightly higher than 7/3 - as it should be in the case of a conservative cascade. With this results on the multifractal spectrum of the dissipation (together with the one found in [14]) the fractal dimension should be lower than 7/3.

5. Conclusions

The invariants of the velocity gradient tensor show the specific topology of the flow in the VSL and TSL within the TNTI and can be described by a simple model unifying the previous models for each separate (sub)layer. With this model knowledge of the eddy characteristics near the TNTI *e.g.* eddy radius R_{eddy} allows the determination of the background strain γ_{eddy} which permits estimating the (mean) values of the invariants across the VSL and TSL, therefore opening the door to the development of new models for the turbulent entrainment mechanism based on the small scale eddies, associated with the 'nibbling' mechanism [16], and to mixing

models for free shear flows, which are often based on the dissipation rate, which is simply $\varepsilon \approx -4\nu Q$ in the VSL. The TNTI provides also an interesting example where the coherent features of the flow are directly linked to the geometrical and dynamical features of the flow.

The analysis of trial functions have shown that the methodology implemented for the analysis of multifractal systems is able to recover the theoretical predictions. By investigating the multifractal spectrum of dissipation in fully-developed turbulence the main result present in [14] was recovered with a different method: the non conservativeness of the multiplicative process which describes energy dissipation. At the interface, evidences that the multifractal spectrum is similar to the turbulent region was found, which is in agreement with the experimental findings of [2] and these results yield a fractal dimension of the interface of about $d_f \approx 2.28$. This issue needs further assessment. The expansion of the method to analyse 3D fields is sufficient to develop a tool to analyse without limitation the multifractal spectrum in the interface, being therefore able to determine the fractal dimension of the interface. The proposed analysis for several different flows will be able to clarify the universality of the interesting results obtained.

Acknowledgements

The author would like to thank to Prof. Carlos B. da Silva and Rodrigo R. Taveira for their great orientation and daily availability to teach, help and discuss. They opened my horizons in this amazing field of science.

References

[1] Carlos B. da Silva, Julian C.R. Hunt, Ian Eames, and Jerry Westerweel. Interfacial layers between regions of different turbulence intensity. *Annual Review of Fluid Mechanics*, 46(1):567–590, 2014.

[2] Charles Meneveau and K. R. Sreenivasan. Interface dimension in intermittent turbulence. *Phys. Rev. A*, 41:2246–2248, Feb 1990.

[3] M. S. Chong, A. E. Perry, and B. J. Cantwell. A general classification of three dimensional flow fields. *Physics of Fluids A: Fluid Dynamics (1989-1993)*, 2(5), 1990.

[4] K. Falconer. *Fractal Geometry - mathematical foundations and applications.* Wiley, 2^{nd} edition, 2003.

[5] U. Frisch G. Parisi. *Turbulence and predictability in geophysical fluid dynamics and climate dynamics*, page 84. North Holland, 1985.

[6] Thomas C. Halsey, Mogens H. Jensen, Leo P. Kadanoff, Itamar Procaccia, and Boris I. Shraiman. Fractal measures and their singularities: The characterization of strange sets. *Phys. Rev. A*, 33:1141–1151, Feb 1986.

[7] Ingrid Daubechies and Jeffrey C. Lagarias. *On the thermodynamic formalism for multifractal functions*, chapter 9, pages 213–264.

[8] Charles Meneveau and K. R. Sreenivasan. The multifractal nature of turbulent energy dissipation. *Journal of Fluid Mechanics*, 224:429, 1991.

[9] C. Meneveau and K. R. Sreenivasan. Simple multifractal cascade model for fully developed turbulence. *Phys. Rev. Lett.*, 59:1424–1427, Sep 1987.

[10] A. Arneodo, E. Bacry, and J.F. Muzy. The thermodynamics of fractals revisited with wavelets. *Physica A: Statistical Mechanics and its Applications*, 213(12):232 – 275, 1995. Proceedings of the Third European Days of Thermodynamics on Inhomogeneous Phases and Pattern Formation.

[11] Stphane Jaffard, Bruno Lashermes, and Patrice Abry. Wavelet leaders in multifractal analysis. In Tao Qian, MangI Vai, and Yuesheng Xu, editors, *Wavelet Analysis and Applications*, Applied and Numerical Harmonic Analysis, pages 201–246. Birkhuser Basel, 2007.

[12] Rodrigo R. Taveira and Carlos B. da Silva. Characteristics of the viscous superlayer in shear free turbulence and in planar turbulent jets. *Physics of Fluids (1994-present)*, 26(2):–, 2014.

[13] A. A. Wray J. Jimenez. On the characteristics of vortex filaments in isotropic turbulence. *Journal of Fluid Mechanics*, 373:255–285, 1998.

[14] Pierre Kestener and Alain Arneodo. Three-dimensional wavelet-based multifractal method: The need for revisiting the multifractal description of turbulence dissipation data. *Phys. Rev. Lett.*, 91:194501, Nov 2003.

[15] R. Ramshankar K. R. Sreenivasan and C. Meneveau. Mixing, entrainment and fractal dimensions of surfaces in turbulent flows. *Proc. R. Soc. Lond. A*, 421:79–108, 1989.

[16] J. Westerweel, C. Fukushima, J. M. Pedersen, and J. C. R. Hunt. Mechanics of the turbulent-nonturbulent interface of a jet. *Phys. Rev. Lett.*, 95:174501, Oct 2005.